Journal of
Intelligent Material
Systems and Structures

Original Article

Journal of Intelligent Material Systems and Structures
2017, Vol. 28(8) 1036–1049
© The Author(s) 2016
Reprints and permissions:
sagepub.co.uk/journalsPermissions.nav
DOI: 10.1177/1045389X16666179
journals.sagepub.com/home/jim
SAGE

Integrated semi-active seat suspension for both longitudinal and vertical vibration isolation

Xian-Xu Bai, Peng Jiang and Li-Jun Qian

Abstract

"Functional integration" is to integrate two or multiple systems or mechanisms that are independent with each other and to realize the two or multiple functions using only one actuation system. Maximization of engineering applications of actuation systems could be achieved through the use of the "functional integration" concept-based structural design. In this article, an integrated semi-active seat suspension, mainly composed of a switching mechanism, a transmission amplification mechanism, and a damping force- or torque-controllable rotary magnetorheological (MR) damper working in pure shear mode, for both longitudinal and vertical vibration attenuation, is proposed, designed, and fabricated. The switching mechanism employs the parallelogram frames as a motion guide which keeps the seat moving longitudinally and vertically. Both longitudinal and vertical motions are transformed into a reciprocating rotary motion that is transmitted to the rotary MR damper after an amplification by a gear mechanism. The torque generated by the MR damper can be tuned by adapting the applied current in real time, and hence, effective two-dimensional vibration control of the seat could be realized. The mathematical model of the semi-active seat suspension system is established, and vibration isolation performance of the system is simulated and analyzed. Based on the established experimental test rig, the prototype of the semi-active seat suspension system is tested, and the results of the mathematical model and the experimental test are compared.

Keywords

Functional integration, seat suspension, magnetorheological fluids, magnetorheological damper, vibration isolation

Introduction

Vibration isolation seat suspensions

Vibrations from vehicles, such as motor vehicles, water vehicles, and aircrafts, due to rough roads, waves, and other excitations, are generally smaller than 10 Hz (Li et al., 2012), which covers the sensitive frequency range of occupant body. When the vibrations transmit to the seats, they would influence riding (driving) comfort for occupants and even lead to their health and security issues (Paddan and Griffin, 2002; Pope et al., 1999; Tong and Amirouche, 1998). Seats, from the view of vibration attenuation, are actually a vibration isolation element installed between the occupants and vehicles. The bottom of the seats is fixed onto the vehicles, while the seat pans support the occupants. Two means or steps could be used to attenuate vibrations transmitted from seats to occupants and improve riding comfort and security performance. On one hand, the vibrations from the vehicles themselves should be controlled so as to control the seat vibrations from the source. On the other hand, the vibration could be attenuated on the way of the vibration transmission by the seat suspensions which connect the seats to the vehicles. Suspensions for ground vehicles are a typical application of the former-mentioned approach, because vibrations due to the road-induced excitations transmitting from tires to the vehicle body can be, to some extent, mitigated by the vehicle suspensions (Bai et al., 2013; Du et al., 2012; Koch et al., 2010; Shafie et al., 2015). However, for ships and aircrafts, it is hard to utilize this approach. In recent years, increasing attentions are paid to how to improve the seat suspension

Laboratory for Adaptive Structures and Intelligent Systems (LASIS), Department of Vehicle Engineering, Hefei University of Technology, Hefei, People's Republic of China

Corresponding author:
Xian-Xu Bai, Laboratory for Adaptive Structures and Intelligent Systems (LASIS), Department of Vehicle Engineering, Hefei University of Technology, Hefei 230009, People's Republic of China.
Email: bai@hfut.edu.cn

performance and isolate the vibrations transmitting to the seats and occupants (Gan et al., 2015; Maciejewski and Krzyżyński, 2011; Tufano and Griffin, 2013).

Seat suspensions could be categorized into passive, active, and semi-active seat suspensions according to control types (Abbas et al., 2013). Passive seat suspensions consisted of springs and hydraulic dampers have advantages of simple configuration and low cost, but the parameters of the springs and the hydraulic dampers are determined by experiential or optimal design and cannot be adjusted to adapt to different working conditions (Choi et al., 2003; Maciejewski et al., 2009). Active seat suspensions provide controllable driving force using hydraulic actuators, pneumatic actuators, or servo motors, and possess excellent vibration control performance. Maciejewski et al. (2010) proposed an active seat suspension system based on a controllable pneumatic spring and a hydraulic damper, and the active control of driving force is implemented by a controller and a proportional valve which could control expansion and compression of the airflow in the pneumatic spring. Stein (1997) developed an electro-pneumatic active seat suspension for a driver's seat for heavy earth moving equipment or off-road vehicles, the seat suspension utilized a pneumatic spring and a proportional electro-pneumatic transducer to provide active driving force. Kawana and Shimogo (1998) proposed an active seat suspension for a heavy-duty truck, the seat suspension uses an electric servo-motor and a ball-screw mechanism to provide controllable driving force. The active seat suspensions show excellent vibration control performance, but their practical applications are restricted due to their complex structure, high power consumption, and also high cost (Kela and Vähäoja, 2009). Semi-active seat suspensions often consist of stiffness-controllable elastic elements or damping-adjustable elements, and they have advantages of simple structure as passive seat suspensions and decent vibration mitigation performance as active seat suspensions. They provide a wide application prospects (Kostamo et al., 2014; Sun et al., 2011; Weber, 2014). Wu and Griffin (1997) developed a semi-active seat suspension using an electrorheological (ER) damper with continuously controllable damping force characteristics. Choi and Wereley (2005) showed that semi-active helicopter crew seat suspensions using magnetorheological (MR) dampers could effectively reduce harm to the occupants induced by impact force. Choi et al. (2000, 2015), Choi and Han (2007), and Shin and Choi (2015) have done much on the applications of ER dampers, MR dampers, and other semi-active actuators used in seat suspensions. Sun et al. (2015) proposed a seat suspension system based on four MR elastomers horizontally installed onto a conventional passive seat suspension that could only adaptively attenuate longitudinal vibration to achieve a half semi-active control for the longitudinal vibration and a half passive control for vertical vibration simultaneously.

New innovation

Up to date, majority of structural designs of the seat suspensions focus on vertical vibration attenuation only. Even some seat suspension structures have two- or multi-dimensional vibration attenuation performance, they are repetitive combinations of several one-dimensional hardwares, and any dimension is completely decoupled with another. These two- or multi-dimensional vibration attenuation seat suspensions will inevitably increase the system installation space, cost, and complexity. The control system should further consider the two or three one-dimensional vibration isolation performances simultaneously and make compromises in between. The complexity of the system control increases tremendously and the system performance and reliability will be influenced.

The "functional integration" concept is summarized from our previous research (Wang and Bai, 2013; Wang et al., 2010; Wang and Wang, 2009). In detail, assuming that one functional system (or mechanism) can only provide one function, "functional integration" is to integrate and simplify two or multiple systems that are independent with each other and to realize the two or multiple functions that originally need repetitive combinations of two or multiple systems with only one actuation system. Although the system coupling may occur and/or even partial function of the integrated system will be sacrificed during integration and simplification, there are at least two particular advantages of the new integrated system based on the "functional integration" concept listed as follows: (i) Only one actuation system is enough to provide two or multiple functions at the same time. The installation space and cost of the system could be effectively decreased via integration and simplification of the hardwares. (ii) The conflicts among the systems originally decoupled with each other could be centralized into the new integrated system and can be coordinately optimized via primary structural design. Complex control, if the two or multiple functions are realized by two or multiple systems decoupled with each other, can be avoided.

As we could imagine, if the "functional integration" concept could be utilized for seat suspension design to realize an integrated two- or multi-dimensional controllable seat suspension system, not only the seat suspension structure could be simplified and the installation space could be tailored, but also the real-time control for two- or multi-dimensional seat vibrations could be coordinately realized. Moreover, it would also further decrease the system cost and maximize the engineering applications of the controllable seat suspension systems.

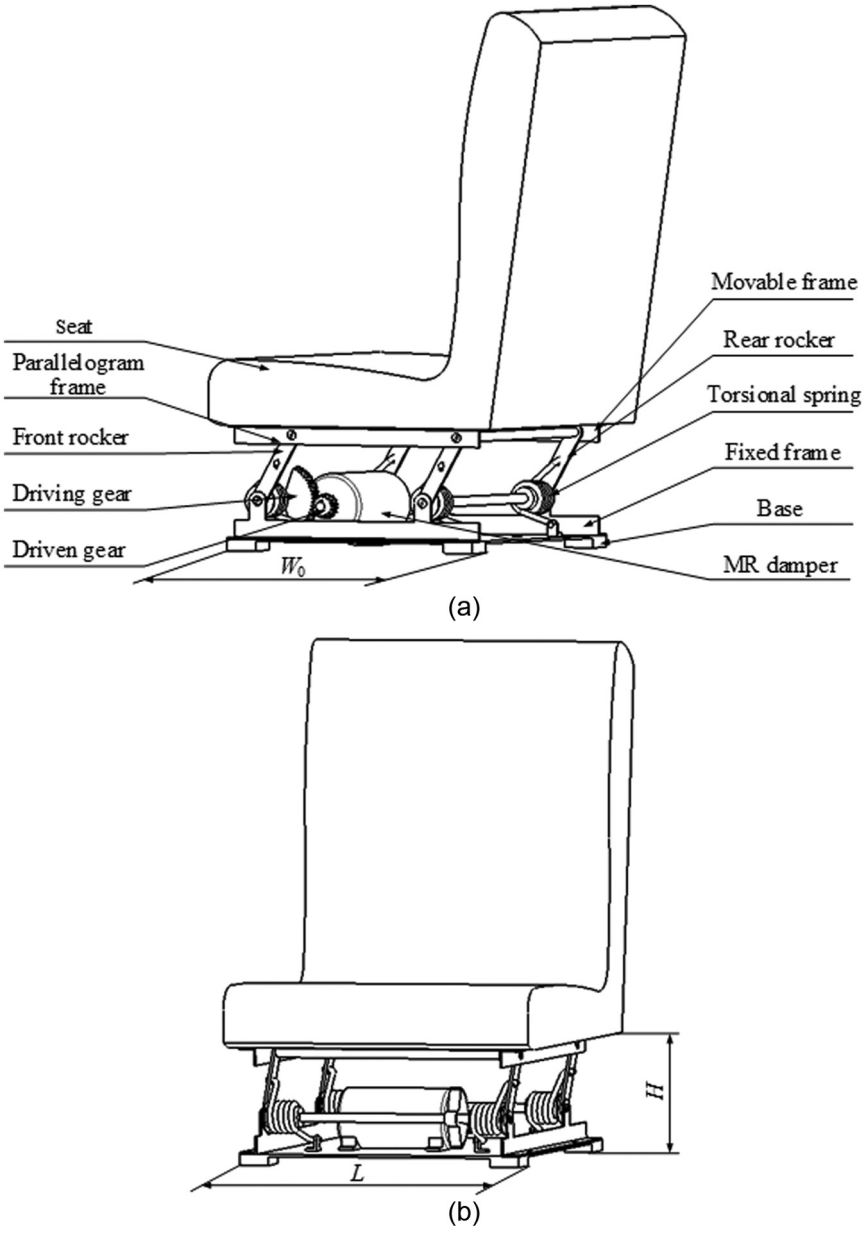


Figure 1. Three-dimensional drawing of the seat suspension system: (a) the side view and (b) the front view.

In this study, an integrated semi-active seat suspension system for both longitudinal and vertical vibration attenuation is proposed. The system transforms both longitudinal and vertical vibrations of the seat into a reciprocating rotary motion by a switching mechanism. The mechanical energy of the longitudinal and vertical vibrations is transmitted to the controllable rotary MR damper and dissipated. The mathematical model of the semi-active seat suspension system is established for theoretical analysis. Based on the established experimental test rig, the vibration control performance of the seat suspension prototype is preliminarily tested and compared with the model-based theoretical results.

Structure and principle of the seat suspension system

Structure of the seat suspension system

Employing the "functional integration" concept, an integrated semi-active seat suspension for both longitudinal and vertical vibration attenuation is proposed. Figures 1(a) and (b) present the side view and front view of the three-dimensional drawing of the seat suspension system, respectively. Figure 2 shows the kinematic principle of the seat suspension system. As shown in Figures 1 and 2, the seat suspension system consists of a motion switching mechanism, a transmission amplification mechanism, a damping force- or torque-

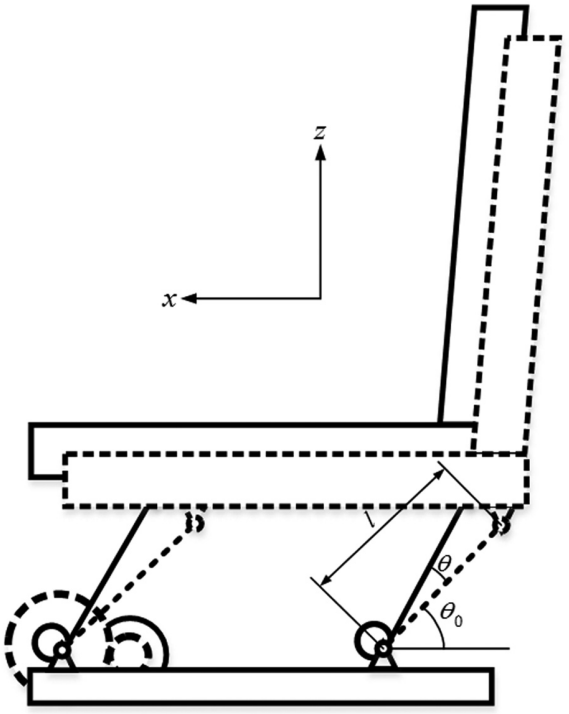


Figure 2. Kinematic principle of the seat suspension system.

controllable actuator, and elastic elements. The switching mechanism is composed of two parallelogram frames with movable frames, front and rear rockers, and fixed frames. The parallelogram frames will guide the seat to move longitudinally (x-axis) and vertically (z-axis) as seen from Figure 2. Meanwhile, the longitudinal and vertical motions of the seat are transformed into a rotatory motion by the parallelogram frames, and the motion transformation function enables the integrated control of both longitudinal and vertical vibrations. The damping force- or torque-controllable actuator is realized by a rotary MR damper working in pure shear mode (Wang and Liao, 2011), which features rapid response and large range of controllable damping force or torque. A pair of driving and driven gears serve as the transmission amplification mechanism. The driving gear rotates with the rockers and transmits both longitudinal and vertical vibrations of the seat to the driven gear that is coupled with the transmission shaft of the rotary MR damper. Consequently, a single actuator (the rotary MR damper) is competent to attenuate two-dimensional (longitudinal and vertical) vibrations. The gear mechanism is also utilized to amplify the rotatory motion of the rockers so as to increase the effective stroke of the rotary MR damper. A total of four torsional springs with the same property are installed between the hinged point of the four rockers and the fixed frames and serve as the elastic elements to support the static weight of the seat and the occupant. The parameters of the torsional spring are listed in Table 1.

Table 1. Parameters of the torsional spring.

Parameter	Symbol	Value	Unit
Nominal torque	T_n	56.2	N m
Working angle	φ	28.1	°
Free angle	φ_0	60	°
Winding ratio	C_r	5	–
Wire diameter	d	9	mm
Pitch diameter	D	40	mm
Number of coils	n_t	4	turn
Stiffness	k_0	2	N m/°

Modeling of the seat suspension system

According to Figures 1 and 2, the dynamics of the seat suspension system can be decomposed into the longitudinal direction (x-axis) and vertical direction (z-axis), and the corresponding schematics of the models are presented in Figures 3(a) and (b), respectively. The dynamic models of the seat suspension system in the longitudinal direction and vertical direction, as can be seen in Figures 3(a) and (b), can be expressed as

$$\begin{cases} m\ddot{x}_2 + \frac{k_x\theta}{l} = F_{\mathrm{MRD}x} \\ x_2 - x_1 = l\cos\theta_0 - l\cos(\theta_0 + \theta) \end{cases} \tag{1a}$$

$$\begin{cases} m\ddot{z}_2 + \frac{k_z\theta}{l} = F_{\mathrm{MRD}z} \\ z_2 - z_1 = l\sin(\theta_0 + \theta) - l\sin\theta_0 \end{cases} \tag{1b}$$

where m is the total mass of the seat and the occupant; k_x ($= k\sin(\theta_0 + \theta)$) is the longitudinal component of the total stiffness (k) of the torsional springs; k_z ($= k\cos(\theta_0 + \theta)$) is the vertical component of the total stiffness (k) of the torsional springs; l is the length of the rocker; θ_0 is the angle between the rocker and the longitudinal direction when the seat is at the static equilibrium state; θ is the rotational angle of the rocker; x_1 and z_1 are the longitudinal and vertical displacement excitations to the seat suspension system, respectively; x_2 and z_2 are the longitudinal and vertical displacement responses of the seat suspension system, respectively; $\ddot{x}_2$ and $\ddot{z}_2$ are the longitudinal and vertical acceleration responses of the seat suspension system, respectively; and $F_{\mathrm{MRD}x}$ and $F_{\mathrm{MRD}z}$ are the longitudinal and vertical components of the damping force generated by the rotary MR damper, respectively. $F_{\mathrm{MRD}x}$ and $F_{\mathrm{MRD}z}$ can be written as

$$F_{\mathrm{MRD}x} = \frac{(n_r)^2 c_{px}\dot{\theta} + n_r T_{\mathrm{MRD}x}}{l} \tag{2a}$$

$$F_{\mathrm{MRD}z} = \frac{(n_r)^2 c_{pz}\dot{\theta} + n_r T_{\mathrm{MRD}z}}{l} \tag{2b}$$

where n_r is the transmission ratio of the gear mechanism; c_{px} ($= c_p\sin(\theta_0 + \theta)$) is the longitudinal component of the equivalent damping (c_p) of the seat suspension system at passive state; c_{pz}

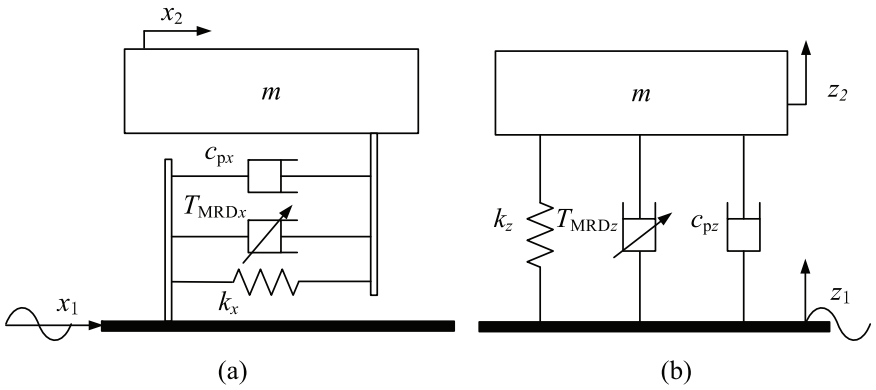


Figure 3. Dynamic models of the seat suspension system: (a) The longitudinal direction and (b) the vertical direction.

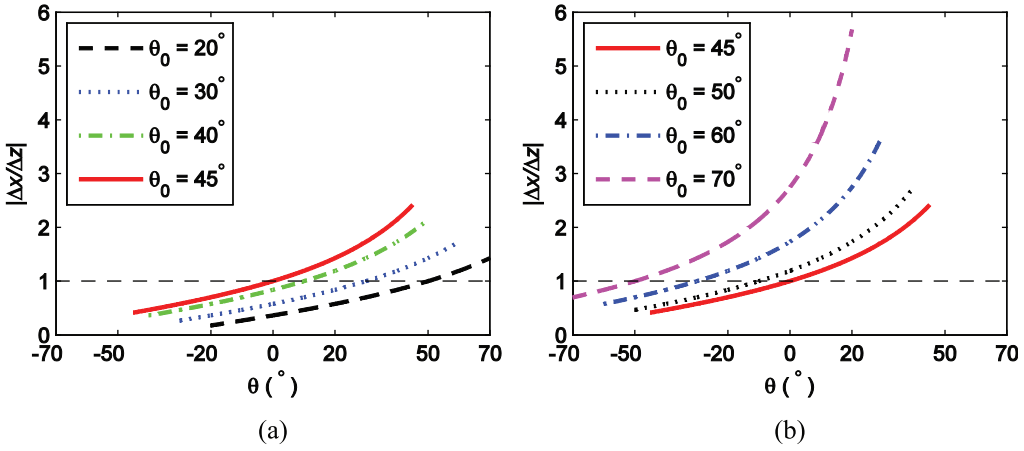


Figure 4. Relationships between the longitudinal displacement (Δx) and the vertical displacement (Δz) with the rotational angle of the rocker (θ), when at different static equilibrium states: (a) $\theta_0 \in (0^\circ, 45^\circ]$ and (b) $\theta_0 \in (45^\circ, 90^\circ)$.

($= c_p \cos(\theta_0 + \theta)$) is the vertical component of the equivalent damping (c_p) of the seat suspension system at passive state; T_{MRDx} ($= T_{MRD} \sin(\theta_0 + \theta)$) is the longitudinal component of the controllable torque (T_{MRD}) generated by the MR damper; T_{MRDz} ($= T_{MRD} \cos(\theta_0 + \theta)$) is the vertical component of the controllable torque (T_{MRD}) generated by the MR damper; and $\dot{\theta}$ is the rotational angular velocity of the rocker.

As shown in Figures 1 and 2, when the seat moves longitudinally (vertically), it will also move vertically (longitudinally) at the same time. Assuming that the counterclockwise direction is the positive direction when the rockers rotate, the absolute value of the longitudinal displacement (Δx) and vertical displacement (Δz) can be respectively expressed as

$$|\Delta x| = |l \cos\theta_0 - l \cos(\theta_0 + \theta)| \tag{3a}$$

$$|\Delta z| = |l \sin(\theta_0 + \theta) - l \sin\theta_0| \tag{3b}$$

The difference $f(\theta_0, \theta)$ and the ratio $g(\theta_0, \theta)$ between the absolute value of $|\Delta x|$ and $|\Delta z|$ can be given by

$$f(\theta_0, \theta) = |\Delta x| - |\Delta z| \tag{4}$$

$$g(\theta_0, \theta) = \left|\frac{\Delta x}{\Delta z}\right| \tag{5}$$

According to equations (3) to (5), the relationships between the longitudinal displacement and the vertical displacement can be obtained by analyzing the relationships between the value of $f(\theta_0, \theta)$ and/or $g(\theta_0, \theta)$ and parameters (θ_0 and θ). This is of importance to make a trade-off between the longitudinal and vertical vibration attenuation performances when designing the seat suspension systems.

Based on equations (3)–(5), Figures 4(a) and (b) present the relationships between $g(\theta_0, \theta)$ and parameters (θ_0 and θ) when $\theta_0 \in (0^\circ, 45^\circ]$ and $\theta_0 \in (45^\circ, 90^\circ)$, respectively. Observing Figure 4(a), when $\theta_0 \in (0^\circ, 45^\circ]$, if $\theta \in [-\theta_0, 2(45^\circ - \theta_0)]$, then $g(\theta_0, \theta) \le 1$ (i.e., $f(\theta_0, \theta) \le 0$), and the vertical displacement is larger than the longitudinal displacement. If $\theta \in (2(45^\circ - \theta_0), 90^\circ - \theta_0]$, then $g(\theta_0, \theta) > 1$ (i.e., $f(\theta_0, \theta) > 0$), and the vertical displacement is smaller

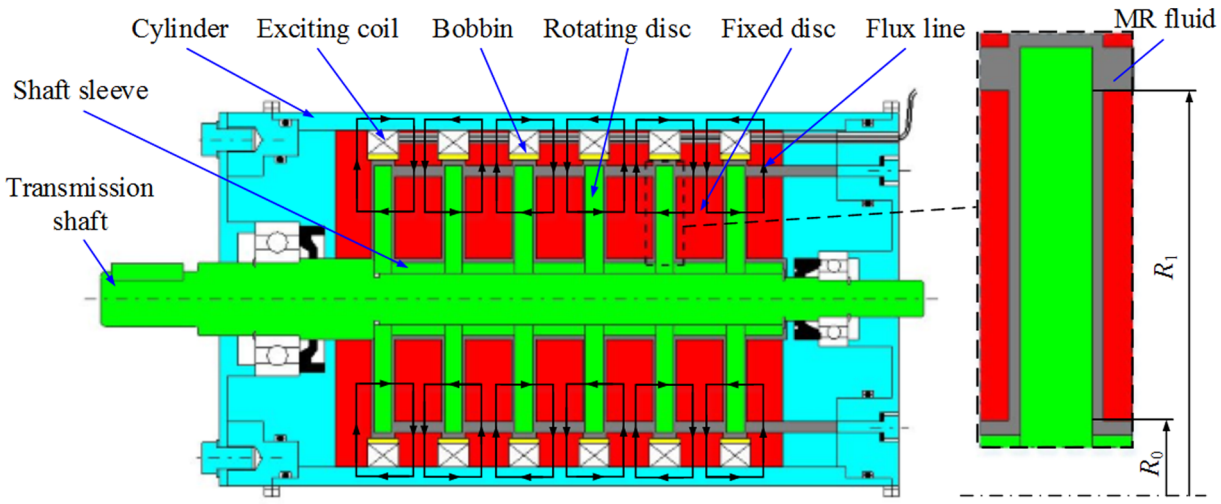


Figure 5. Structure of the rotary MR damper.

than the longitudinal displacement. As shown in Figure 4(a), when $g(\theta_0, \theta) \leq 1$, the smaller the θ_0, the larger the rotational angle (θ) range, and the vertical displacement is larger than the longitudinal displacement when the rockers rotate within this rotational range. When $g(\theta_0, \theta) > 1$, the smaller the θ_0, the smaller the rotational angle (θ) range, and the longitudinal displacement is larger than the vertical displacement when the rockers rotate within this rotational range.

Observing Figure 4(b), when $\theta_0 \in (45°, 90°)$, if $\theta \in [-2(\theta_0 - 45°), 90° - \theta_0]$, then $g(\theta_0, \theta) \geq 1$ (i.e., $f(\theta_0, \theta) \geq 0$), and the vertical displacement is smaller than the longitudinal displacement. If $\theta \in [-\theta_0, -2(\theta_0 - 45°))$, then $g(\theta_0, \theta) < 1$ (i.e., $f(\theta_0, \theta) < 0$), and the vertical displacement is larger than the longitudinal displacement. As shown in Figure 4(b), when $g(\theta_0, \theta) > 1$, the greater the θ_0, the larger the rotational angle (θ) range, and the longitudinal displacement is larger than the vertical displacement when the rockers rotate within this rotational range. When $g(\theta_0, \theta) \leq 1$, the larger the θ_0, the smaller the rotational angle (θ) range, and the vertical displacement is larger than the longitudinal displacement when the rockers rotate within this rotational range.

According to equations (1)–(4) and Figure 4, a compromise between the longitudinal and vertical vibration displacements can be made by adjusting the static equilibrium state (selecting θ_0). Furthermore, combining equations (1) and (2), the vibration attenuation of the seat suspension system can be realized when in different working conditions (no matter whether the longitudinal displacement is larger than the vertical displacement or the opposite situation) via the real-time control of the damping force or torque of the rotary MR damper.

Modeling of the rotary MR damper

MR dampers using a smart material, MR fluids, can provide controllable damping force by tuning magnetic fields (Bai et al., 2015). Figure 5 shows the structural principle of a rotary MR damper designed for the proposed seat suspension system. As seen from Figure 5, the MR damper consists of fixed parts, rotating parts, and filled MR fluids. The fixed parts composed of fixed discs and bobbins are static relative to the cylinder. The rotating parts, including the transmission shaft, the rotating discs, and the shaft sleeves, rotate relatively to the fixed parts. The bobbins are fixed between two adjacent fixed discs. MR fluids fill the space formed by the fixed discs, rotating discs, bobbins, and shaft sleeves and work in pure shear mode. To ensure reasonable controllable damping force or torque performance of the MR damper, the fixed discs, the rotating discs, and the cylinder are all made from the materials with high permeability, and the others are made from nonmagnetic materials. The magnetic field generated by the exciting coils with applied current starts from the cylinder, passes through the coil-left fixed disc, the MR fluids between the coil-left fixed disc and the rotating disc, the rotating disc, the MR fluids between the coil-right fixed disc and the rotating disc, and the coil-right fixed disc, and finally closes at the cylinder, as shown in Figure 5. The specific advantage of the proposed rotary MR damper featuring pure shear mode is that the damping force or torque is nearly independent of the excitation speeds. In other words, large dynamic range that is defined by the ratio of the field-controlled damping force or torque to the passive damping force or torque can be achieved.

When no magnetic field, MR fluids behave as Newtonian fluids. In the presence of the magnetic field generated by the exciting coils with applied current,

MR fluids show a characteristic of Bingham fluids (Olabi and Grunwald, 2007). Ignoring the torque generated by mechanical friction, the total torque T_0 produced by a single pair of rotating-fixed discs can be expressed as

$$T_0 = T_\eta + T_m \tag{6}$$

where T_η is the torque dependent on the viscosity of the MR fluids and T_m is the torque dependent on the magnetic flux density. T_η and T_m can be, respectively, expressed as

$$T_\eta = 2\pi\eta\dot{\gamma}\int_{R_0}^{R_1} r^2 dr \tag{7a}$$

$$T_m = 2\pi\tau_y(B)\int_{R_0}^{R_1} r^2 dr \tag{7b}$$

where η is the viscosity of the MR fluids; $\dot{\gamma}$ is the shear rate; R_0 and R_1 are the inner radius of the fixed disc and outer radius of the rotating disc, respectively; and $\tau_y(B)$ is the shear yield stress related to the magnetic field and is given by

$$\tau_y(B) = k_1 B^\alpha \tag{8}$$

where k_1 and α are the fitting coefficients and B is the magnetic flux density.

From equations (6)–(8), damping force or torque of the MR damper will be increased (or decreased) by increasing (or decreasing) the magnetic flux density. Combining equations (1) and (2), dynamic response of the seat could be controlled by tuning the applied current to the MR damper in real time.

To validate the magnetic principle of the proposed rotary MR damper, the software package ANSYS Maxwell is used to simulate the electromagnetic characteristics of the MR damper. Figures 6(a) and (b) present the magnetic flux density contours and the magnetic flux lines when a current level of 3 A is applied to the MR damper. As shown in Figure 6(a), the magnetic flux density between the fixed discs and the rotating discs is nearly 0.3 T. As seen from Figure 6(b), the magnetic flux lines travel through two adjacent fixed discs, the rotating disc between two adjacent fixed discs, and the cylinder, which validates the principle of the MR damper shown in Figure 5.

Numerical simulation

In order to theoretically analyze the performance of the proposed seat suspension system, MATLAB/Simulink is utilized to simulate the vibration transmissibility of the seat suspension system when the MR damper provides passive-on torques. Sinusoidal swept-frequency displacement excitations with an amplitude of 15 mm and a frequency range of 0.5–6 Hz are applied to the seat suspension system. The parameters of the seat suspension model are listed in Table 2.

Figures 7(a) and (b) present very similar acceleration responses in the longitudinal and vertical directions of the seat suspension system. As shown in Figure 7, the acceleration transmissibility at passive state (the equivalent damping (c_p) of the MR damper is around 0.0322 N m s/°) is greater than those when under passive-on states ($T_{MRD}>0$). As T_{MRD} increases, the acceleration transmissibility decreases. Meanwhile, the resonance frequency of the seat suspension system increases with the increase in T_{MRD}, which results from nonlinear characteristics of the stiffness according to equations (2a) and (2b). Furthermore, combining Figure 4, relationships between longitudinal and vertical displacements of the seat will transform with the change of θ, and this will lead to variable values of the ratio of longitudinal (vertical) force to the total spring force. When the excitation frequency is below 3.5 Hz, the greater the controllable torque (T_{MRD}) is, the smaller the acceleration transmissibility will be. Increasing the torque generated by the rotary MR damper will effectively suppress the acceleration transmissibility when near the resonance frequency. When the excitation frequency is above 3.5 Hz, the smaller the controllable torque (T_{MRD}) is, the smaller the acceleration transmissibility. In other words, according to the feedback signals via the dynamic sensors for the excitations applied to the base of the seat suspension or dynamic response of the seated occupants, the real-time integrated semi-active control for both longitudinal and vertical vibrations of the seat suspension system can be realized by controlling the applied current to the MR damper (i.e., controlling the T_{MRD}).

In addition, the sensitive frequency ranges of human body in the longitudinal and vertical directions are 1–2 and 4–8 Hz (International Organization for Standardization, 1997), respectively. Thence, the resonance frequency range (2.5–3.0 Hz) of the designed seat suspension system, in this study, is kept away from the sensitive frequencies of human body, as shown in Figures 7(a) and (b).

Experimental investigation

Rotary MR damper

Figure 8 presents the established torque-test rig for the rotary MR damper. To obtain the torque controllability of the MR damper, the MR damper under different excitation speeds (n) of 15, 60, and 180 r/min within a safe current range (0–4 A) is tested.

Figures 9(a) and (b) present the controllable torque range and dynamic range of the MR damper. As shown in Figure 9(a), when no applied current, the torque

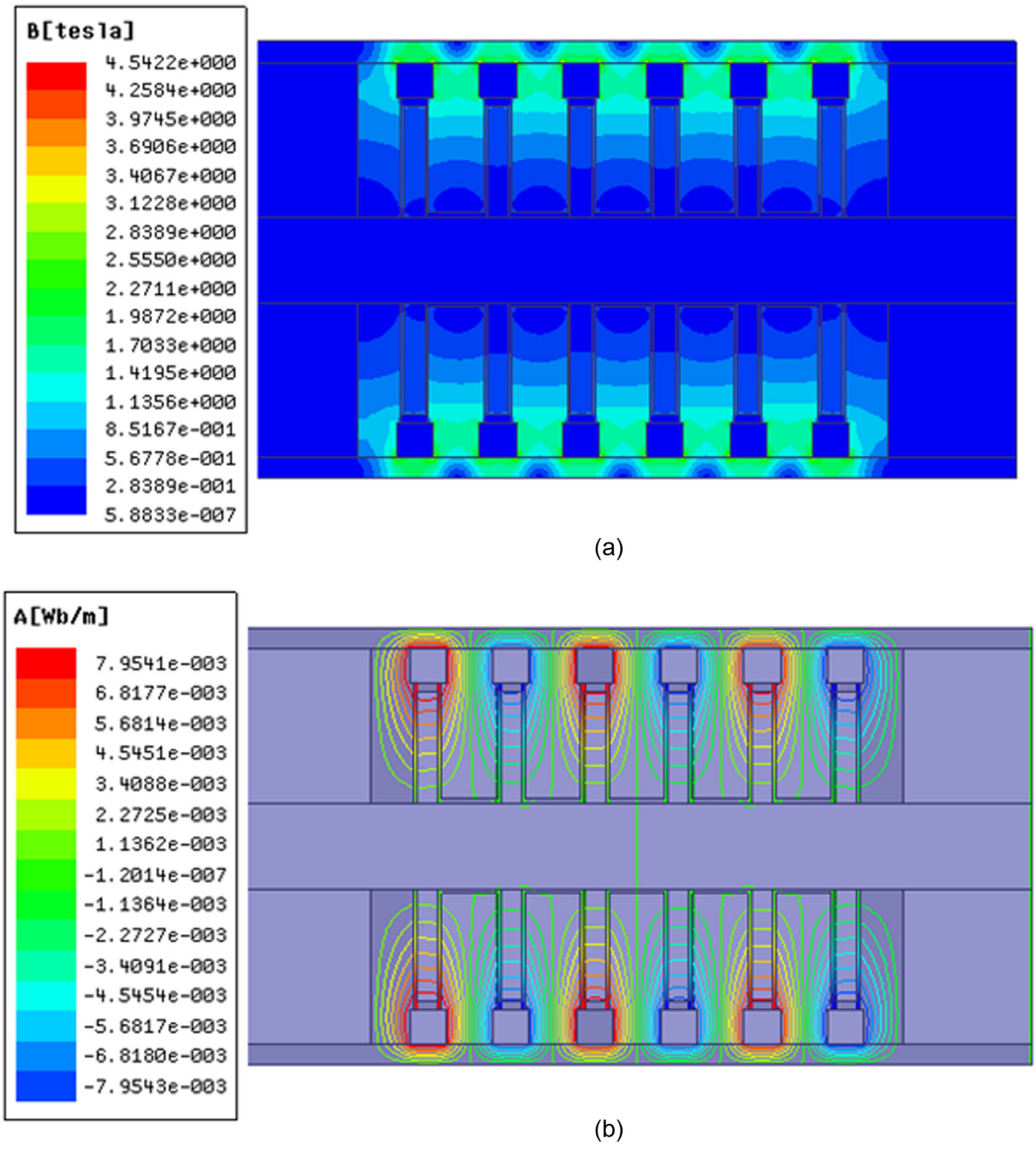


Figure 6. Magnetic field of the rotary MR damper: (a) the magnetic flux density contours and (b) the magnetic flux lines.

generated by the MR damper is around 1.02 N m, while with a maximum current of 4 A, the maximum torque increases to around 13.53 N m. The torque approximately increases linearly with the increase of the applied current. Observing Figure 9(b), the dynamic range of the MR damper increases with the increase of the applied current and is as high as over 8 when applied with a maximum current of 4 A. The increase of the excitation speed will slightly influence the dynamic range of the MR damper, and similar result can be seen in Figure 9(a). The developed rotary MR damper can be potentially applied into high-speed impact control systems.

Vibration isolation test of the seat suspension system

Figure 10 presents the vertical vibration test rig for the seat suspension system. As shown in Figure 10, the seat suspension system is installed on the vibration actuator, and a mass of 77 kg representing a Hybrid III 50th male (National Highway Traffic Safety Administration, 2013) is fixed onto the seat. Two accelerometers (Type: DYTRAN3035B) are respectively set on the seat and the base of the seat suspension to measure vertical accelerations. A data acquisition system (Type: DEWE-501, not shown in this figure) is employed to acquire and process the acceleration signals.

Table 2. Parameters of the seat suspension model.

Parameter	Symbol	Value	Unit
Total mass of the seat and occupant	m	97	kg
Total stiffness of the torsional springs	k	8	N m/°
Controllable torque generated by the rotary MR damper	T_{MRD}	–	N m s/°
Equivalent damping of the seat suspension system at passive state	c_p	0.0322	N m s/°
Length of the rocker	l	120	mm
Angle between the rocker and the longitudinal direction when the seat is at the static equilibrium state	θ_0	50.7	°
Rotational angle of the rocker	θ	–	°
Transmission ratio of the gear mechanism	n_r	3	–
Length of the seat suspension	L	430	mm
Width of the seat suspension	W_0	495	mm
Height of the seat suspension when the seat is at the static equilibrium state	H	180	mm

MR: magnetorheological.

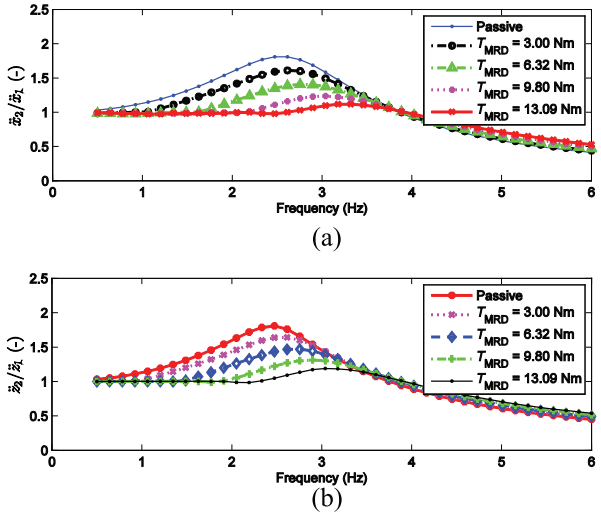


Figure 7. Numerical simulation results of the seat suspension system: (a) acceleration transmissibility in the longitudinal direction and (b) acceleration transmissibility in the vertical direction.

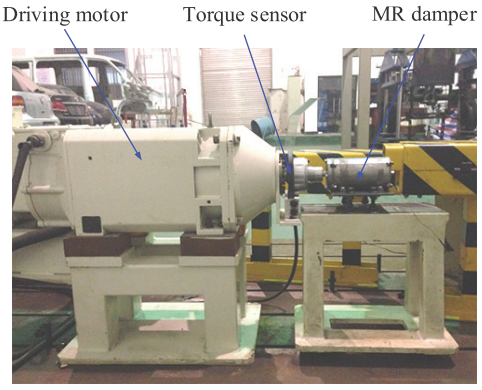


Figure 8. Torque-test rig for the rotary MR damper.

Figure 11 presents the acceleration transmissibility of the seat suspension system when sinusoidal displacement excitations with an amplitude of 15 mm and a frequency range of 0.5–5 Hz are applied to the base of the seat suspension, and the applied currents are 0, 1, 2, 3, and 4 A. Figures 12–14 present the time histories of the acceleration responses of the seat when sinusoidal displacement excitations with an amplitude of 15 mm and frequencies of 1.5, 2.4, and 3.5 Hz are applied to the base of the seat suspension and different applied currents, respectively. Figure 15 presents the time histories of the acceleration response of the seat when a sinusoidal displacement excitation with an amplitude of 15 mm and a frequency of 2.4 Hz is applied to the base of the seat suspension, and the applied current is 0–4 A. It should be noted that in this study, for the rotary MR damper of the developed seat suspension system, the applied current of 0 A corresponds to an equivalent damping value 0.0322 N m s/° (i.e., when the seat suspension system at passive state), and the applied currents of 1, 2, 3, and 4 A correspond to the controllable torque (T_{MRD}) values of 3.00, 6.32, 9.80, and 13.09 Nm, respectively.

Observing Figure 11, the acceleration transmissibility of the seat suspension system decreases with the increase of applied current. Combining Figure 7(b), the increase of the applied current (i.e., increase of T_{MRD}) presents obvious effect on the acceleration transmissibility near the resonance frequency (2.4–2.7 Hz). When the excitation frequency is >2.7 Hz, the smaller the applied current, the better the vibration isolation. The resonance frequency of the seat suspension system obtained from the experiments increases with the increase of T_{MRD}, the applied current of 0 A corresponds to the passive state of the system. Comparing Figures 7(b) and 11, the resonance frequency range (2.4–2.7 Hz) obtained from the experiments is approximate to the theoretical results (2.5–3.0 Hz). However, the acceleration transmissibility near resonance frequency shows a slight difference, as seen from Figures 7(b) and 11, and the difference will decrease with

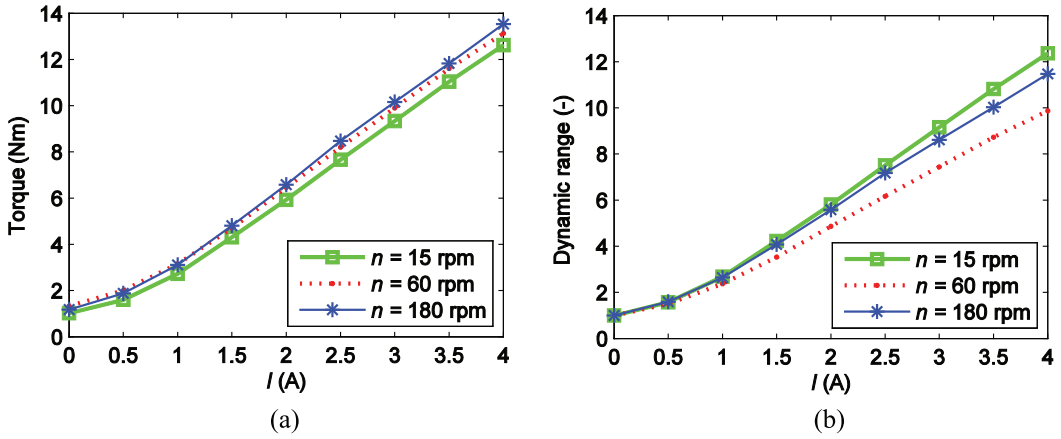


Figure 9. Performance of the rotary MR damper: (a) the controllable torque range and (b) the dynamic range.

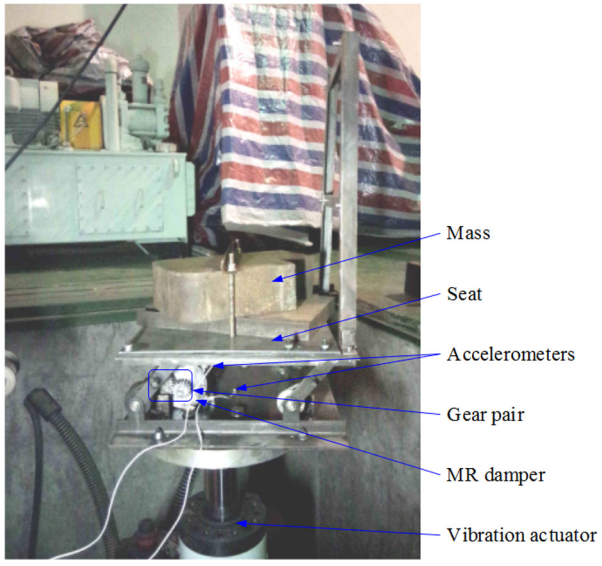


Figure 10. Vertical vibration test rig for the seat suspension system.

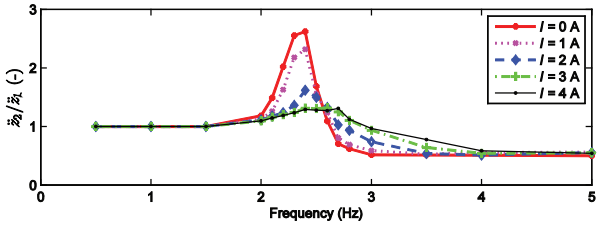


Figure 11. Acceleration transmissibility of the seat suspension system when sinusoidal displacement excitations with an amplitude of 15 mm and a frequency range of 0.5–5 Hz are applied to the base of the seat suspension, and the applied currents are 0, 1, 2, 3, and 4 A.

increasing the applied current. This is related to the effect of "double-frequency vibration" of the seat suspension during the experimental test.

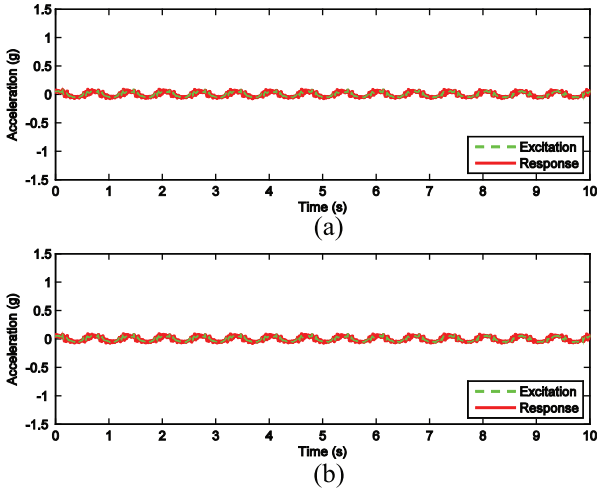


Figure 12. Time histories of the acceleration response of the seat suspension when a sinusoidal displacement excitation with an amplitude of 15 mm and a frequency of 1.5 Hz is applied to the base of the seat suspension: (a) I = 0 A and (b) I = 3 A.

As shown in Figures 12(a) and (b), when the excitation frequency is 1.5 Hz, the acceleration response of the seat at applied current of 0 A is nearly the same as that at applied current of 3 A. Due to the mechanical friction of the developed seat suspension system, small excitation acceleration can hardly drive the seat to response as it should be in theory and the seat almost remains static relative to the excitation actuator. As shown in Figures 13(a) and (b), when the excitation frequency (2.4 Hz) approaches to the resonance frequency of the seat suspension system, the seat acceleration decreases with the increase of the applied current. When the excitation frequency is 3.5 Hz, both the seat accelerations at applied currents of 0 and 3 A are smaller than the excitation acceleration and increase with the increase of the applied current, as presented in Figures 14(a) and (b). When very near the resonance frequency of the seat suspension system, as can be seen

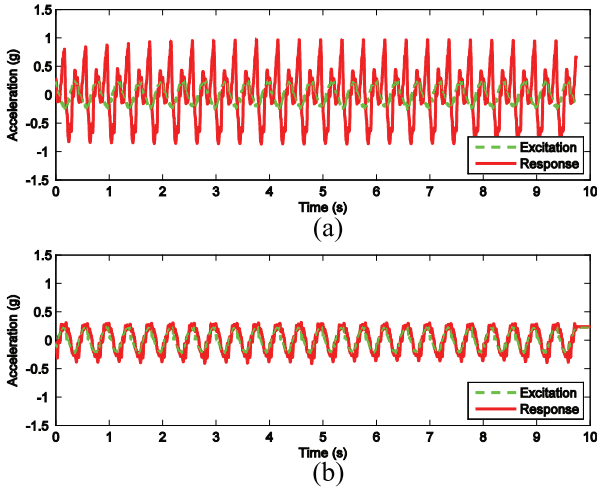


Figure 13. Time histories of the acceleration response of the seat suspension when a sinusoidal displacement excitation with an amplitude of 15 mm and a frequency of 2.4 Hz is applied to the base of the seat suspension: (a) I = 0 A and (b) I = 3 A.

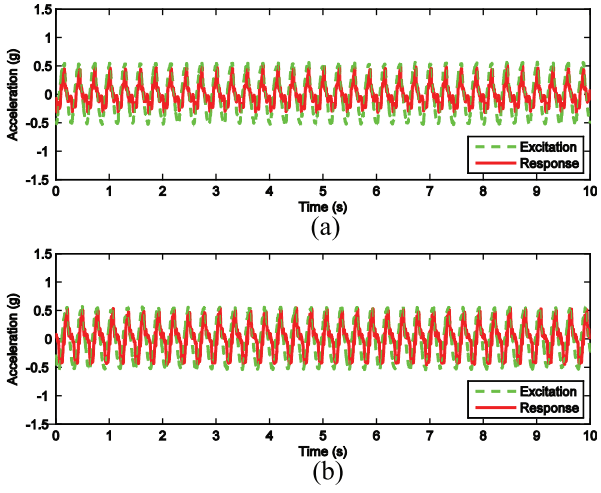


Figure 14. Time histories of the acceleration response of the seat suspension when a sinusoidal displacement excitation with an amplitude of 15 mm and a frequency of 3.5 Hz is applied to the base of the seat suspension: (a) I = 0 A and (b) I = 3 A.

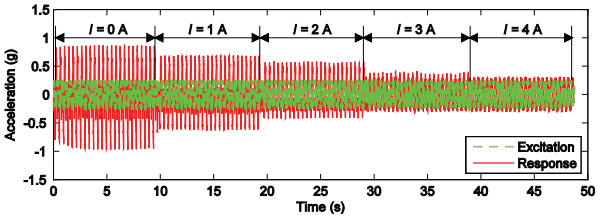


Figure 15. Time histories of the acceleration response of the seat suspension when a sinusoidal displacement excitation with an amplitude of 15 mm and a frequency of 2.4 Hz is applied to the base of the seat suspension.

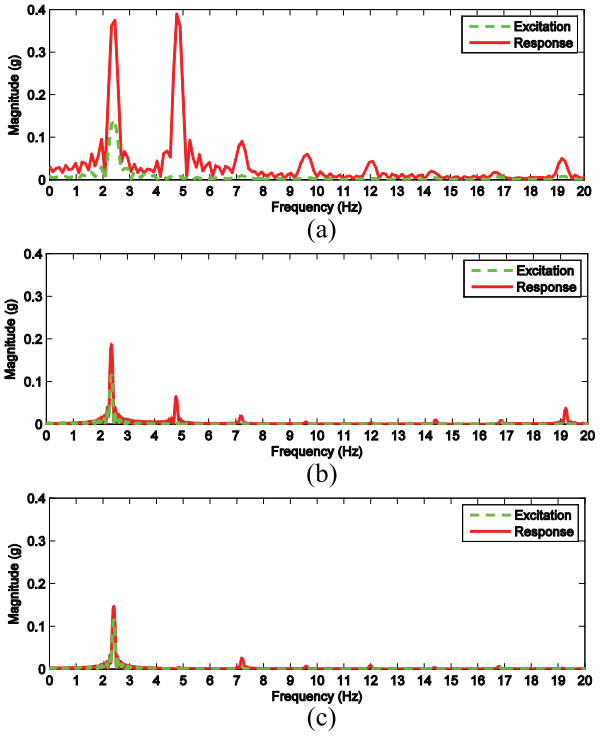


Figure 16. Frequency-domain signals obtained via FFT for the time-domain signals when a sinusoidal displacement excitation with an amplitude of 15 mm and a frequency of 2.4 Hz is applied to the base of the seat suspension: (a) I = 0 A, (b) I = 2 A, and (c) I = 4 A.

from Figure 15, the greater the applied current is, the smaller the seat acceleration is, which indicates that the vibration control can be realized by tuning the applied current.

As shown in Figures 12–15, the acceleration transmissibility directly calculated from the time-domain signals is greater than that presented in Figure 11. This is because the mass and the seat are not a rigid body, and to different extents, there are impacts between them when conducting the experiments. To further explain the influence of the impacts, fast Fourier transformation (FFT) is implemented for the time-domain signals in this study. The acceleration transmissibility of the seat suspension system in the whole frequency range (0.5–5 Hz) as shown in Figure 11 is obtained by fitting the calculated transmissibility (the ratio of the response magnitude to excitation magnitude at the fundamental frequency) from the FFT results.

Figures 16(a)–(c) partly present the frequency-domain signals obtained via FFT for the time-domain signals, which are acquired when a sinusoidal displacement excitation with an amplitude of 15 mm and a frequency of 2.4 Hz is applied to the base of the seat suspension, and the applied currents are 0, 2, and 4 A. As shown in Figure 16(a), when the applied current is 0 A, magnitude at the double frequency (4.8 Hz) is very high, which is caused by two impacts between the

mass and the seat during one cycle of the fundamental frequency (one at the wave crest and the other at the wave trough), the phenomenon is the "double-frequency vibration." The influence of the impacts weakens with the increase in the applied current, and the magnitude at the double frequency (4.8 Hz) decreases too, as shown in Figures 16(b) and (c), when the applied currents are 2 and 4 A, respectively. It implies that the difference between the acceleration transmissibility obtained from the experiments and the numerical simulation will decrease with the increase of the applied current, as also seen from Figures 7(b) and 11.

As it can be seen from Figures 11–15, by controlling the applied current to the MR damper, passive-on control of vertical vibration of the seat suspension system can be realized. According to equations (3)–(5), there is a specific relationship between longitudinal and vertical displacements (also the accelerations) of the seat suspension system. That is to say, if the vertical vibration transmission characteristics are verified, the longitudinal vibration transmission characteristics are also reasonable. In addition, combining the results of numerical simulation presented in Figure 7(b), semi-active control of both longitudinal and vertical vibrations can be realized by the seat suspension system designed based on the MR damper.

Conclusion

In this article, an integrated semi-active seat suspension, consisted of a switching mechanism transforming both longitudinal and vertical motions into a rotary motion and a real-time damping force- or torque-controllable rotary MR damper working in pure shear mode, for both longitudinal and vertical vibration attenuation was proposed, designed, and manufactured. The switching mechanism employs the parallelogram frames as a motion guide which keeps the seat moving longitudinally and vertically. Both longitudinal and vertical motions are transformed into a reciprocating rotary motion which is transmitted to the rotary MR damper after an amplification by a gear mechanism. The mathematical model of the seat suspension system was established in MATLAB/Simulink, and the vibration control performance of the system was simulated and analyzed. The vibration control performance of the seat suspension prototype was preliminarily tested and compared to the model-based theoretical results. Based on the research results, concluding remarks could be obtained as follows:

(i) Passive-on control of both longitudinal and vertical vibrations of the seat suspension system can be realized through applying constant currents to the MR damper. When near the resonance frequency of the seat suspension system, the increase of the applied current to the MR damper is of help to attenuate both longitudinal and vertical vibrations, while when over the transmissibility-cross frequency, smaller applied current is better for vibration attenuation. As a result of the nonlinear coupling characteristics of the system, the phenomenon of "double-frequency vibration" appears in the experiments, which will be solved in the next experiments by optimizing the structural materials of the seat suspension system. The research work on the semi-active control of the desired torque of the developed MR damper for the seat suspension system for both longitudinal and vertical vibration control will be undertaken in the near future.

(ii) A trade-off between the longitudinal and vertical vibration displacements (dynamic responses) can be made by adjusting the static equilibrium state (by selecting θ_0), which is the design foundation for the seat suspension system according to the practical application environment.

(iii) Within a certain current range (0–4 A), the torque of the MR damper featuring pure shear mode increases almost linearly from 1.02 to 13.53 N m, and its dynamic range can be as high as over 8 when under different excitation speeds. The field-dependent torque of the MR damper is nearly independent of the excitation speeds, which enables the developed rotary MR damper to be applied to high-speed vibration or impact control systems.

The realized integrated two-dimensional controllable seat suspension system, employing the concept of "functional integration," has demonstrated that not only the seat suspension structure can be simplified and the installation space can be decreased, but also the real-time coordinated control of two-dimensional seat vibrations can be realized. Moreover, it would also further decrease the two-dimensional system cost and maximize the engineering applications of the controllable seat suspension systems. "Functional integration" concept-based structural designs are of significance and help for multi-dimensional actuation or control systems to simplify the structures and control the volumes and the cost.

Acknowledgements

The authors would like to thank Mr Hui Pan, a Bachelor student from Hefei University of Technology, for his assistance in design and finite element analysis of the rotary MR damper.

Declaration of Conflicting Interests

The author(s) declared no potential conflicts of interest with respect to the research, authorship, and/or publication of this article.

Funding

The author(s) disclosed receipt of the following financial support for the research, authorship, and/or publication of this article: This work was supported by the National Natural Science Foundation of China (Grant no. 51305114), Anhui Provincial Natural Science Foundation (Grant no. 1408085QE91), and Fundamental Research Funds for the Central Universities (no. 2014HGCH0008).

References

Abbas W, Emam A, Badran S, et al. (2013) Optimal seat and suspension design for a half-car with driver model using genetic algorithm. *Intelligent Control and Automation* 4(2): 199–205.

Bai XX, Hu W and Wereley NM (2013) Magnetorheological damper utilizing an inner bypass for ground vehicle suspensions. *IEEE Transactions on Magnetics* 49(7): 3422–3425.

Bai XX, Wereley NM and Hu W (2015) Maximizing semi-active vibration isolation utilizing a magnetorheological damper with an inner bypass configuration. *Journal of Applied Physics* 117(17): 17C711.

Choi SB and Han YM (2007) Vibration control of electrorheological seat suspension with human-body model using sliding mode control. *Journal of Sound and Vibration* 303(1–2): 391–404.

Choi SB, Choi JH, Lee YS, et al. (2003) Vibration control of an ER seat suspension for a commercial vehicle. *Journal of Dynamic Systems, Measurement and Control* 125(1): 60–68.

Choi SB, Lee YS and Han MS (2015) Vibration control of a vehicle's seat suspension featuring a magnetorheological damper based on a new adaptive fuzzy sliding-mode controller. *Proc IMechE, Part D: J Automobile Engineering*. Epub ahead of print 10 June. DOI: 10.1177/0954407015586678.

Choi SB, Nam MH and Lee BK (2000) Vibration control of a MR seat damper for commercial vehicles. *Journal of Intelligent Material Systems and Structures* 11(12): 936–944.

Choi YT and Wereley NM (2005) Biodynamic response mitigation to shock loads using magnetorheological helicopter crew seat suspensions. *Journal of Aircraft* 42(5): 1288–1295.

Du H, Li W and Zhang N (2012) Integrated seat and suspension control for a quarter car with driver model. *IEEE Transactions on Vehicular Technology* 61(9): 3893–3908.

Gan Z, Hillis A and Darling J (2015) Adaptive control of an active seat for occupant vibration reduction. *Journal of Sound and Vibration* 349: 39–55.

International Organization for Standardization (1997) Mechanical vibration and shock-evaluation of human exposure to whole-body vibration-Part 1: general requirements (2631–1: 1997).

Kawana M and Shimogo T (1998) Active suspension of truck seat. *Shock and Vibration* 5(1): 35–41.

Kela L and Vähäoja P (2009) Recent studies of adaptive tuned vibration absorbers/neutralizers. *Applied Mechanics Reviews* 62(6): 060801.

Koch G, Fritsch O and Lohmann B (2010) Potential of low bandwidth active suspension control with continuously variable damper. *Control Engineering Practice* 18(11): 1251–1262.

Kostamo E, Focchi M, Guglielmino E, et al. (2014) Magnetorheologically damped compliant foot for legged robotic application. *Journal of Mechanical Design* 136(2): 021003-1–021003-11.

Li W, Zhang X and Du H (2012) Development and simulation evaluation of a magnetorheological elastomer isolator for seat vibration control. *Journal of Intelligent Material Systems and Structures* 23(9): 1041–1048.

Maciejewski I and Krzyżyński T (2011) Control design of semi-active seat suspension systems. *Journal of Theoretical and Applied Mechanics* 49(4): 1151–1168.

Maciejewski I, Meyer L and Krzyżyński T (2009) Modelling and multi-criteria optimization of passive seat suspension vibro-isolating properties. *Journal of Sound and Vibration* 3–5: 520–538.

Maciejewski I, Meyer L and Krzyżyński T (2010) The vibration damping effectiveness of an active seat suspension system and its robustness to varying mass loading. *Journal of Sound and Vibration* 329(19): 3898–3914.

National Highway Traffic Safety Administration (2013) Federal motor vehicle safety standard No. 208: occupant crash protection. US Department of Transportation, Title 49, Subtitle B, Chapter V, Part 571.

Olabi AG and Grunwald A (2007) Design and application of magneto-rheological fluids. *Materials & Design* 28(10): 2658–2664.

Paddan GS and Griffin MJ (2002) Evaluation of whole-body vibration in vehicle. *Journal of Sound and Vibration* 253(1): 195–213.

Pope MH, Wilder DG and Magnusson ML (1999) A review of studies on seated whole body vibration and low back pain. *Proc IMechE, Part H: J Engineering in Medicine* 213(6): 213–435.

Shafie AA, Bello MM and Khan RM (2015) Active vehicle suspension control using electro hydraulic actuator on rough road terrain. *Journal of Advanced Research* 9(1): 15–30.

Shin DK and Choi SB (2015) Design of a new adaptive fuzzy controller and its application to vibration control of a vehicle seat installed with an MR damper. *Smart Materials and Structures* 24(8): 085012.

Stein GJ (1997) A driver's seat with active suspension of electro-pneumatic type. *Journal of Vibration and Acoustics* 119(2): 230–235.

Sun SS, Yang J, Deng HX, et al. (2015) Horizontal vibration reduction of a seat suspension using negative changing stiffness magnetorheological elastomer isolators. *International Journal of Vehicle Design* 68(1–3): 104–118.

Sun W, Li J, Zhao Y, et al. (2011) Vibration control for active seat suspension systems via dynamic output feedback with limited frequency characteristic. *Mechatronics* 21(1): 250–260.

Tong RT and Amirouche F (1998) Truck cab suspension design: optimization and vibration control. *International Journal of Heavy Vehicle Systems* 5(3–4): 3–4.

Tufano S and Griffin MJ (2013) Nonlinearity in the vertical transmissibility of seating: the role of the human body apparent mass and seat dynamic stiffness. *Vehicle System Dynamics* 51(1): 122–138.

Wang DH and Bai XX (2013) A magnetorheological damper with an integrated self-powered displacement sensor. *Smart Materials and Structures* 22(7): 075001.

Wang DH and Liao WH (2011) Magnetorheological fluids dampers: a review of parametric modelling. *Smart Materials and Structures* 20(2): 023001.

Wang DH and Wang T (2009) Principle, design and modeling of an integrated relative displacement self-sensing magnetorheological damper based on electromagnetic induction. *Smart Materials and Structures* 18(9): 095025.

Wang DH, Bai XX and Liao WH (2010) An integrated relative displacement self-sensing magnetorheological damper: prototyping and testing. *Smart Materials and Structures* 19(10): 075001.

Weber F (2014) Semi-active vibration absorber based on real-time controlled MR damper. *Mechanical Systems and Signal Processing* 46(2): 272–288.

Wu X and Griffin MJ (1997) A semi-active control policy to reduce the occurrence and severity of end-stop impacts in a suspension seat with an electrorheological fluids damper. *Journal of Sound and Vibration* 203(5): 781–793.

Appendix 1

Notation

B	magnetic flux density
c_{p}	equivalent damping of the seat suspension system at passive state
c_{px}	longitudinal component of the equivalent damping of the seat suspension system at passive state
c_{pz}	vertical component of the equivalent damping of the seat suspension system at passive state
C_{r}	winding ratio of the torsional spring
d	wire diameter of the torsional spring
D	pitch diameter of the torsional spring
$F_{\mathrm{MRD}x}$	vertical component of the damping force generated by the rotary MR damper
$F_{\mathrm{MRD}z}$	longitudinal component of the damping force generated by the rotary MR damper
H	height of the seat suspension when the seat is at the static equilibrium state
I	applied current to the coil of the rotary MR damper
k	total stiffness of the torsional springs
k_x	longitudinal component of the total stiffness of the torsional springs
k_z	vertical component of the total stiffness of the torsional springs
k_0	stiffness of one torsional spring
k_1, α	fitting coefficients for the shear yield stress of the MR fluids related to magnetic fields
l	length of the rocker
L	length of the seat suspension
m	total mass of the seat and occupant
n_{r}	transmission ratio of the gear mechanism
n_{t}	number of coils of the torsional spring
R_0	inner radius of the fixed disc
R_1	outer radius of the rotating disc
T_0	total torque generated by a single pair of rotating-fixed discs of the rotary MR damper
T_{m}	torque dependent on the magnetic flux density of the rotary MR damper
T_{MRD}	total controllable torque generated by the rotary MR damper
$T_{\mathrm{MRD}x}$	longitudinal component of the controllable torque generated by the rotary MR damper
$T_{\mathrm{MRD}z}$	vertical component of the controllable torque generated by the rotary MR damper
T_{n}	nominal torque of the torsional spring
T_η	torque dependent on the viscosity of the MR fluids
W_0	width of the seat suspension
x_1	longitudinal displacement excitation to the seat suspension system
x_2	longitudinal displacement response of the seat suspension system
$\ddot{x}_2$	longitudinal acceleration response of the seat suspension system
z_1	vertical displacement excitation to the seat suspension system
z_2	vertical displacement response of the seat suspension system
$\ddot{z}_2$	vertical acceleration response of the seat suspension system
$\dot{\gamma}$	shear rate
$\lvert\Delta x\rvert$	absolute value of the longitudinal displacement of the seat
$\lvert\Delta z\rvert$	absolute value of the vertical displacement of the seat
η	viscosity of the MR fluids
θ	rotational angle of the rocker
θ_0	angle between the rocker and the longitudinal direction when the seat is at the static equilibrium state
$\tau_{\mathrm{y}}(B)$	shear yield stress of the MR fluids related to magnetic fields
φ	working angle of the torsional spring
φ_0	free angle of the torsional spring